FISEVIER

Contents lists available at ScienceDirect

Journal of Alloys and Compounds

journal homepage: www.elsevier.com/locate/jalcom



Formation mechanism of ceramic/metal composite spherical magnetic abrasive prepared via gas-solid atomization



Linzhi Jiang^a, Tieyan Chang^b, Guixiang Zhang^a,*, Yugang Zhao^a, Haoxin Chen^a, Ning Liu^a, Xue Liu^a

ARTICLE INFO

Article history:
Received 23 May 2022
Received in revised form 16 July 2022
Accepted 19 July 2022
Available online 21 July 2022

Keywords: Ceramic/metal composite spherical magnetic abrasive Gas-solid atomization Breaking mechanism Formation mechanism

ABSTRACT

In order to prepare good magnetic abrasive particles (MAPs) and make it play a better role in magnetic abrasive finishing (MAF), an experimental investigation on the formation mechanism of Al_2O_3 /Fe-based composite spherical MAPs prepared via gas-solid atomization is presented. The morphology of MAPs and the distribution of Al_2O_3 abrasives inside and outside the iron matrix were characterized by scanning electron microscopy and energy-dispersive spectroscopy. The breaking mechanism of gas-solid two-phase flow to molten metal was analyzed by comparing with the metal powder prepared via gas atomization. The formation mechanism of MAPs was studied by analyzing and calculating the mutual movement and cooling process between Al_2O_3 abrasive and metal droplet. The results show that the breaking mechanism of gas-solid two-phase flow to molten metal is quite different from that of pure gas. Under the same experimental conditions, the average particle size of MAPs prepared by gas-solid atomization is smaller than that of metal powders prepared by gas atomization. After observing the surface and cross-section of MAP, it is found that Al_2O_3 abrasives are only evenly and densely distributed on the surface of iron matrix, and there is almost no Al_2O_3 abrasives inside the iron matrix. The calculation shows that in the process of MAPs' formation, the time of Al_2O_3 abrasive moving from the inside to the surface of the droplet is less than that of droplet cooling.

© 2022 Elsevier B.V. All rights reserved.

1. Introduction

Magnetic abrasive finishing (MAF) is a special precision-finishing technology that drives magnetic abrasive particles (MAPs) to finish the surface of parts through the magnetic force generated by magnetic pole [1–3]. Due to the flexibility and self-adaptability of MAPs in the machining process, MAF is mostly used in areas those are not easy to be finished by traditional grinding, such as complex curved surfaces and inner surfaces of parts [4–6]. As a finishing tool, the preparation methods of MAPs include mechanical mixing, sintering, plasma powder melting, gas-solid atomization, etc., among which sintering and mechanical mixing are the main methods [7–10].

In order to give full play to the machining advantages of MAPs, the ideal MAP model should be spherical, and the ceramic abrasives are evenly and densely distributed on the surface of iron matrix, and there are no ceramic abrasives inside the iron matrix (Fig. 1) [11]. The

* Corresponding author. E-mail address: zhanggx@sdut.edu.cn (G. Zhang). ideal MAPs will not only enhance the processing efficiency and uniformity of MAF, but also provide high strength and long processing life for the iron matrix of MAPs, which are not easy to damage in MAF [12]. Sintering and mechanical mixing have simple preparation process and low cost, but the prepared MAPs are often irregular in shape; ceramic abrasives are distributed inside and outside the iron matrix; and the bond formed between ceramic abrasives and iron matrix is not strong, which are far from the ideal MAPs [13,14].

We have successfully prepared Al₂O₃, SiC, CBN, PCD/Fe-based composite spherical MAPs by gas-solid atomization, which are close to the ideal MAP model. They are used in MAF of stainless steel, 718 and other materials, and the MAPs show good processing efficiency and uniformity [15–18]. In the process of MAF, the ceramic abrasives and the iron matrix are firmly combined, and there are almost no ceramic abrasives shedding and iron matrix breaking. The finishing life of MAPs can reach 120 min. Although we have prepared MAPs close to the ideal MAP model, their formation mechanism has not been explored. Sajjadi et al. prepared A356 composite reinforced with Al₂O₃ particles by a developed compocasting method and studied the dispersion process of Al₂O₃ particles in the matrix [19].

^a School of Mechanical Engineering, Shandong University of Technology, Zibo 255000, China

^b NSF's ChemMatCARS, The University of Chicago, Lemont, IL 60439, USA

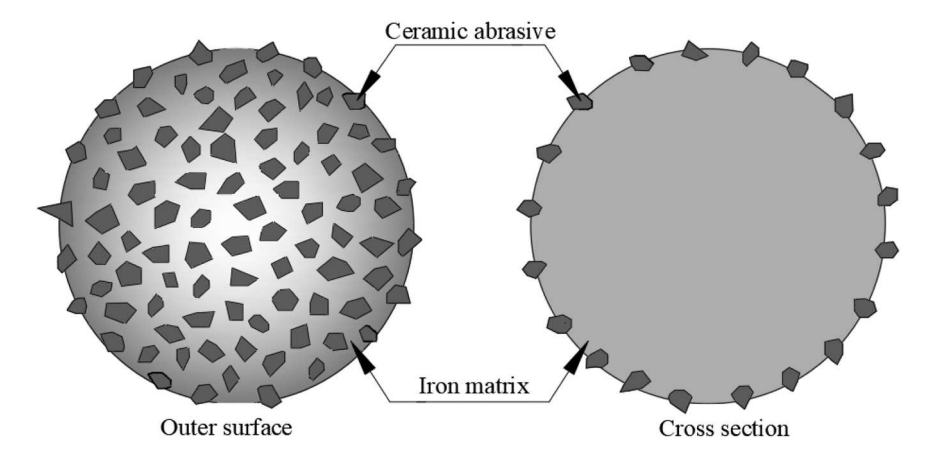


Fig. 1. Ideal model of MAP.

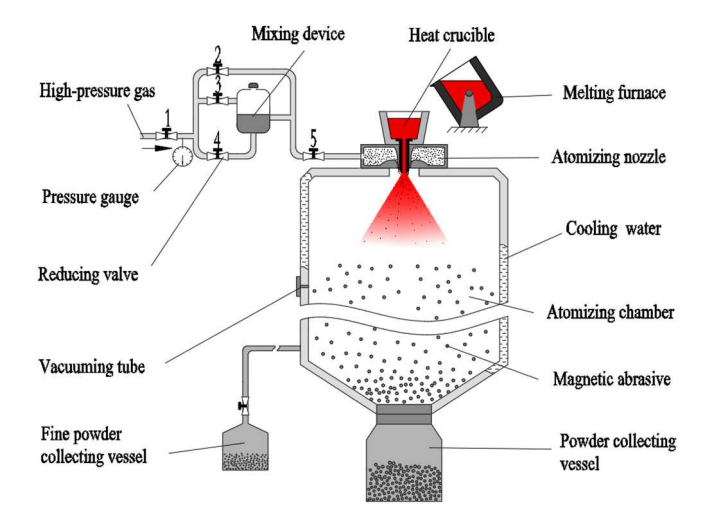
Ao et al. investigated the degradation mechanism of 6063 aluminum matrix composites reinforced with TiC and Al_2O_3 particles and found that the adding of TiC and Al_2O_3 particles reduces the corrosion resistance of the composite material [20]. Gupta et al. prepared metal matrix nanocomposites using Fe as base material reinforced with Al_2O_3 and doped with CeO_2 by powder metallurgy technique and found that 1.0 % CeO_2 doped Fe- Al_2O_3 metal matrix nanocomposite system showed the formation of nano amorphous layer on the specimen surface [21]. We will study the formation mechanism of MAP by analyzing the movement process of Al_2O_3 particles in iron matrix.

In this paper, an investigation on the formation mechanism of ceramic/metal composite spherical MAPs prepared via gas-solid atomization is presented. Compared with the experiment of preparing metal powder via gas atomization, the breaking mechanism of gas-solid two-phase flow to molten metal was analyzed. The formation mechanism of ceramic/metal composite droplets was studied by analyzing the movement process of ceramic abrasives in metal droplets and the cooling process of composite droplets. It provides a theoretical basis for the better development of ceramic/metal composite spherical MAPs prepared via gas-solid atomization.

2. Experiment procedures

MAP consists of iron matrix and ceramic abrasives. The iron matrix had the following composition (in wt%): Si_{9.6}-Al_{5.4}-Ni₅-Fe₈₅. The abrasive phase used in the experiment was Al₂O₃ abrasives (99.99 % pure) with grain sizes of W7 $(5-7 \mu\text{m})$. The atomization gas was N₂. Fig. 2 presents a schematic diagram of the ceramic/metal composite spherical MAP-preparation system. First, the Al₂O₃ abrasives were added to the mixing device, which was connected to the atomizing nozzle and the N_2 cylinder respectively. The iron matrix material was added into the melting furnace and heated to 1650 °C. Then, the molten iron matrix was poured into the heat crucible, while the mixing device was opened at the same time. The falling metal flow was blown and atomized into Al₂O₃/Fe-based composite droplets by N2 mixed with Al2O3 abrasives sprayed from the atomizing nozzle. Finally, the composite droplets were cooled and solidified during the falling process to form Al₂O₃/Fe-based composite spherical MAPs. In order to study the crushing mechanism of gassolid two-phase flow to molten metal, a group of control experiments of preparing metal powders via gas were added. Except that the atomizing medium was replaced by pure N2, other experimental conditions were the same.

To investigate the breaking mechanism of gas-solid two-phase flow to molten metal, the particle size distribution of MAPs prepared by gas-solid atomization and gas atomization was counted and compared. The distribution of Al_2O_3 abrasives on the surface and



 $\textbf{Fig. 2.} \ \ \textbf{Schematic diagram of ceramic/metal spherical MAPs preparation system.}$

inside of iron matrix was observed by scanning electron microscopy (SEM). The distribution of Fe and Al on the surface of MAPs was detected using energy-dispersive spectroscopy (EDS) to analyze and calculate the movement process of Al_2O_3 abrasives in metal droplets. The secondary dendrite arm spacing of MAPs was measured to estimate the cooling rate of composite droplets and determine the formation mechanism of the MAPs. The formation mechanism of MAPs was finally determined by exploring the movement and cooling process.

3. Results and discussion

3.1. Breaking mechanism of gas-solid two-phase flow to molten metal

Fig. 3 shows the Al_2O_3/Fe -based composite spherical MAPs prepared via gas-solid atomization. It can be seen that the MAP exhibits considerable sphericity, and the Al_2O_3 abrasives are uniformly and densely distributed on the surface of iron matrix, which is basically consistent with the ideal MAP model. Fig. 4 shows the comparison of particle size distribution of powders prepared by gas-solid atomization and gas atomization under the same experiment conditions. The average particle size of MAPs prepared by gas-solid atomization is smaller than that of metal powder prepared by gas atomization, which shows that gas-solid two-phase flow has stronger breaking ability to molten metal.

When the atomizing medium impacts the molten metal, the inertial force of the atomizing medium is the fundamental factor to

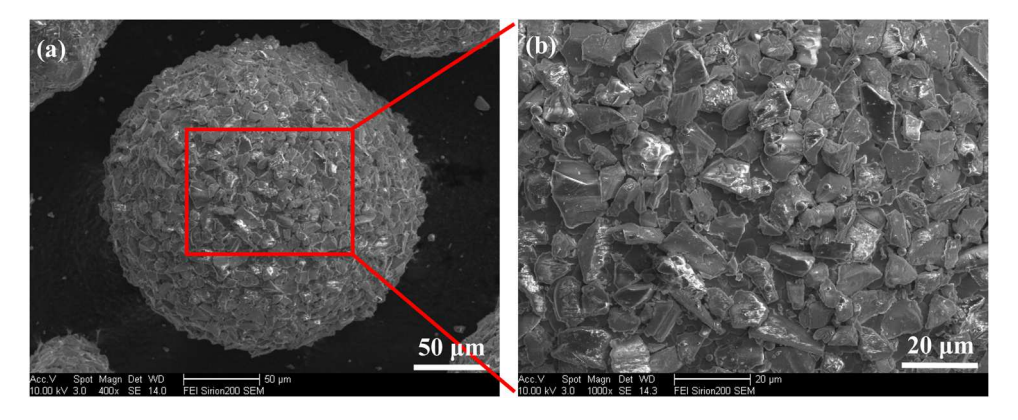


Fig. 3. SEM images of Al₂O₃/Fe-based composite spherical MAP prepared via gas-solid atomization.

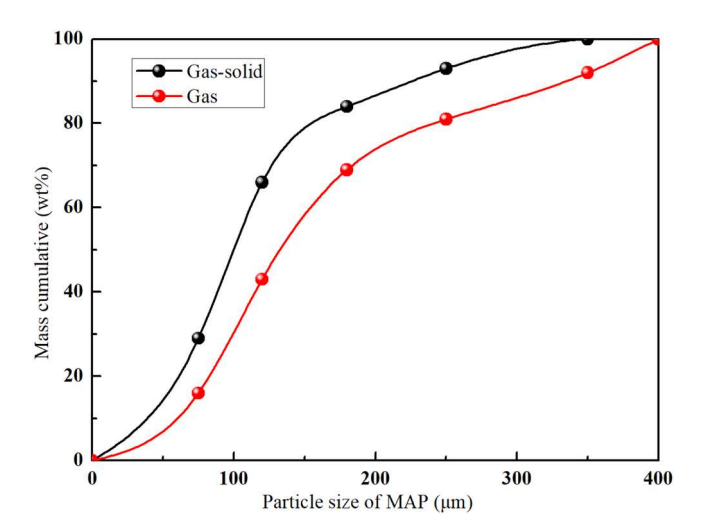


Fig. 4. Particle size distribution of powders prepared by gas-solid atomization and gas atomization.

break the molten metal. When pure gas impacts molten metal, its inertia force is very small due to the extremely small mass of gas molecules. In this case, the gas molecule cannot penetrate the metal liquid surface, but only destabilize the surface through the disturbance energy of gas [22]. The metal droplets get rid of the

bondage of viscous force and separate from the liquid surface to break the molten metal (Fig. 5a). When the gas-solid two-phase flow impacts molten metal, the inertia force of Al_2O_3 abrasives is much greater than that of gas molecules because the mass of Al_2O_3 abrasives is much greater than that of gas molecules. When the gas disturbs the surface of molten metal, it is accompanied by the process of Al_2O_3 abrasives penetrating the surface of molten metal, which makes the molten metal easier to be broken (Fig. 5b).

Weber number (W_e) is the main parameter to measure the degree of droplet breakage in gas atomization [23]. When the Weber number of atomizing medium is greater than a certain critical value, the droplets begin to break. The larger Weber number is, the shorter breaking time and the smaller breaking particle size will be. The Weber number can be expressed as [24]:

$$We = 2\rho g (v_g - v_l)^2 \eta / \sigma_l \tag{1}$$

where ρ_g is the gas density, v_g is the gas velocity, v_l is the droplet velocity, r_l is the droplet radius, and σ_l is the surface tension of the droplet. Due to the low viscosity of molten metal, the metal droplets are mainly affected by aerodynamic force and surface tension. When aerodynamic force and surface tension of metal droplets are in equilibrium [25]:

$$\frac{1}{2}R_l\rho g(\nu_g - \nu_l)^2\pi\eta^2 = 2\pi\eta\sigma_l \tag{2}$$

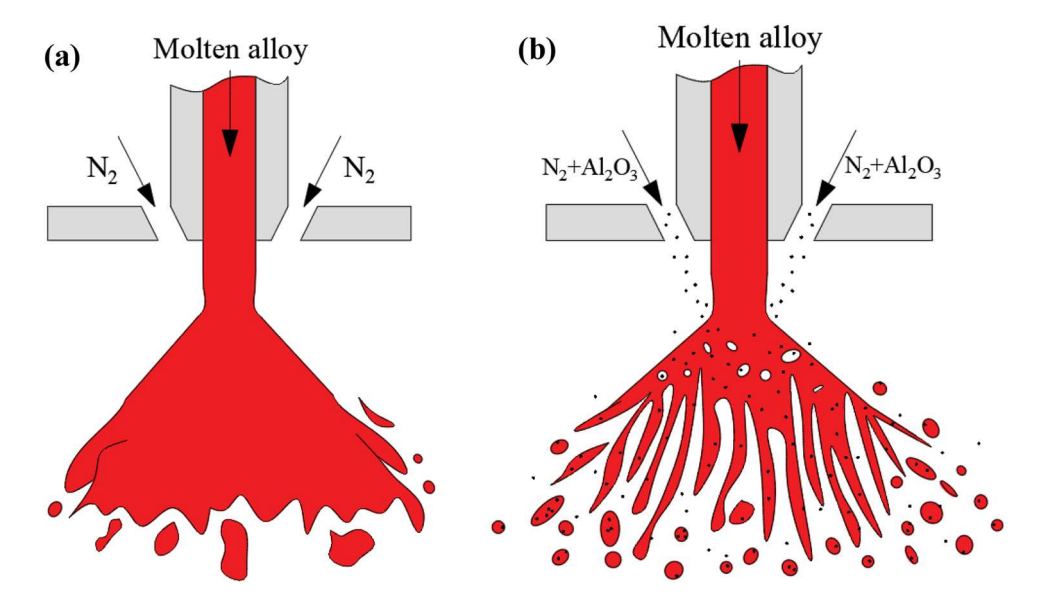


Fig. 5. Schematic diagram of molten metal impacted by different atomizing media: (a) N₂, (b) N₂₊Al₂O₃.

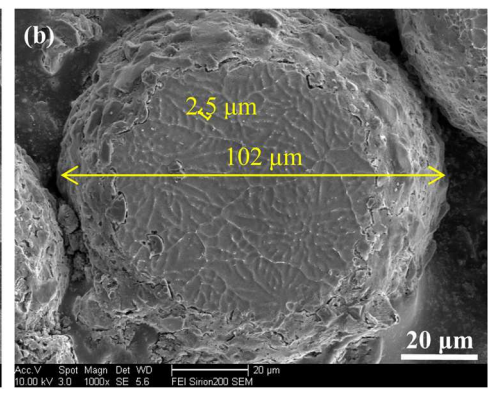


Fig. 6. Cross-sectional pictures of Al₂O₃/Fe-based composite spherical MAPs: (a) Multiple MAPs, (b) Single MAP.

where R_l is the resistance coefficient of metal droplets. The following equation can be obtained by combining Eq. (1) and Eq. (2):

$$We = \frac{2\rho g (v_g - v_l)^2 \eta}{\sigma_l} = \frac{8}{R_l}$$
(3)

In the process of breaking molten metal by gas-solid two-phase flow, metal droplets are affected not only by aerodynamic force and surface tension, but also by the collision force of ceramic abrasives. The abrasive collision force (F_s) per unit time can be expressed as:

$$F_{\rm S} = \rho {\rm SVS}(v_{\rm S} - v_{\rm I}) \tag{4}$$

where ρ_s is the density of Al₂O₃ abrasive, V_s is the volume of Al₂O₃ abrasive, and v_s is the velocity of Al₂O₃ abrasive. Then the critical equation of metal droplet breakage is:

$$\frac{1}{2}R_{l}\rho g(v_{g'}-v_{l})^{2}\pi \eta^{2} + \rho sVs(v_{s}-v_{l}) = 2\pi \eta \sigma_{l}$$
(5)

The following equation can be obtained by combining Eq. (3) and Eq. (5):

$$\frac{2\rho g (v_g'-v_l)^2 \eta}{\sigma_l} + \frac{4\rho s V s (v_s-v_l)}{\pi \eta \sigma_l R_l} = \frac{8}{R_l} \tag{6}$$

Comparing Eq. (3) with Eq. (6), it can be seen that $v_g' < v_g$. That is, when the same metal droplet is broken by different atomizing medium, the velocity of gas-solid two-phase flow is smaller than that of pure gas. In other words, when the velocity of gas-solid two-phase flow is the same as that of pure gas, the breaking effect of gas-solid two-phase flow on metal droplets is better.

3.2. Formation mechanism of ceramic/metal composite spherical MAP

Fig. 6 shows the cross-sectional picture of Al₂O₃/Fe-based composite spherical MAPs prepared via gas-solid atomization. It can be seen from Fig. 6a that some Al₂O₃ abrasives on the surface of MAPs forcibly separated from the phenolic resin remain in the phenolic resin, and there are almost no Al₂O₃ abrasives inside the MAPs embedded in the phenolic resin. It is further revealed that Al₂O₃ abrasives are mostly embedded on the surface of MAP, which is similar to the ideal MAP model. The cross-sectional picture of the MAP after corrosion is shown in Fig. 6b. The average spacing of secondary dendrite arms of MAP with particle size of 102 μm is about 2.5 μm .

Fig. 7 shows the EDS results of MAP surface, in which four main elements of Al, Fe, Si and Ni are detected. It can be seen that most Al_2O_3 abrasives on the surface of MAP are partially covered by iron matrix, and a few Al_2O_3 abrasives are completely covered by iron matrix. It can be inferred that there are two reasons for the phenomenon of Al_2O_3 abrasives partially covered by iron matrix in the atomization process. One is that some Al_2O_3 abrasives float out of the droplet surface soon after entering the droplet interior in the

early stage of metal droplet cooling, and the other is that the remaining Al_2O_3 abrasives fail to break through the droplet surface due to insufficient dynamics. The phenomenon of Al_2O_3 abrasives completely covered by iron matrix is because that they enter the interior of the droplet in the middle and late stage of droplet cooling, and the droplet has solidified when they are about to float out of the surface of the droplet.

When Al_2O_3 abrasives collide with metal droplet, the following three situations may occur. First, the Al_2O_3 abrasives fail to break through the metal droplet surface and stick to or fall off the droplet surface. Second, the Al_2O_3 abrasives are captured by the droplet and move together after entering the metal droplet. Third, the Al_2O_3 abrasives continue to move after entering and penetrating the metal droplet. The first two situations occur when the relative velocity between Al_2O_3 abrasives and metal droplet is low or the internal resistance of droplet is large. The third situation occurs when the relative velocity is high or the internal resistance is small.

When Al_2O_3 abrasive collides with metal droplet, the kinetic energy (ΔE_s) of the Al_2O_3 abrasive changes as follows:

$$\Delta E s = \frac{1}{2} \rho s V s \Delta v_s^2 \tag{7}$$

where Δv_s is the velocity difference before and after Al_2O_3 abrasive collide with the surface of metal droplet.

When Al_2O_3 abrasive enter metal droplet, the surface energy (ΔE_I) of metal droplet changes as follows [25]:

$$\Delta El = -S_s \sigma_l \cos \theta \tag{8}$$

where S_s is the surface area of Al_2O_3 abrasive, and θ is the wetting angle between Al_2O_3 abrasive and metal droplet. When $\Delta E_s - \Delta E_l < 0$, the Al_2O_3 abrasive cannot break through the surface of metal droplet. When $\Delta E_s - \Delta E_l \ge 0$, the Al_2O_3 abrasive enter the metal droplet and move with the droplet or penetrate the droplet. Generally, the Al_2O_3 abrasive's entering and penetrating the droplet should meet the following relationship [26]:

$$1 - 0.246 \left(\frac{2\eta_{\rho_{s}}|\eta_{s} - \eta_{l}|}{\eta_{l}} \right)^{0.407} \left(\frac{2\eta_{\rho_{s}}\sigma_{l}}{\eta_{l}} \right)^{-0.096} \left(\frac{\eta_{l}}{r_{s}} \right)^{-0.278} < 0$$
 (9)

where η_s is the dynamic viscosity of Al₂O₃ abrasive, η_l is the dynamic viscosity of metal droplet, and r_s is the radius of Al₂O₃ abrasive.

Assuming that both Al_2O_3 abrasive and metal droplet are spherical, when Al_2O_3 abrasive cannot penetrate the metal droplet and stays inside the droplet, it is mainly affected by three forces: gravity (F_g) , buoyancy (F_b) and internal friction resistance (F_f) . Fig. 8 shows the force analysis diagram of Al_2O_3 abrasive in the metal droplet.

The gravity (F_g) of Al_2O_3 abrasive can be expressed as:

$$F_g = \rho_s V_s g = \frac{4}{3} \pi \rho_s g r_s^3 \tag{10}$$

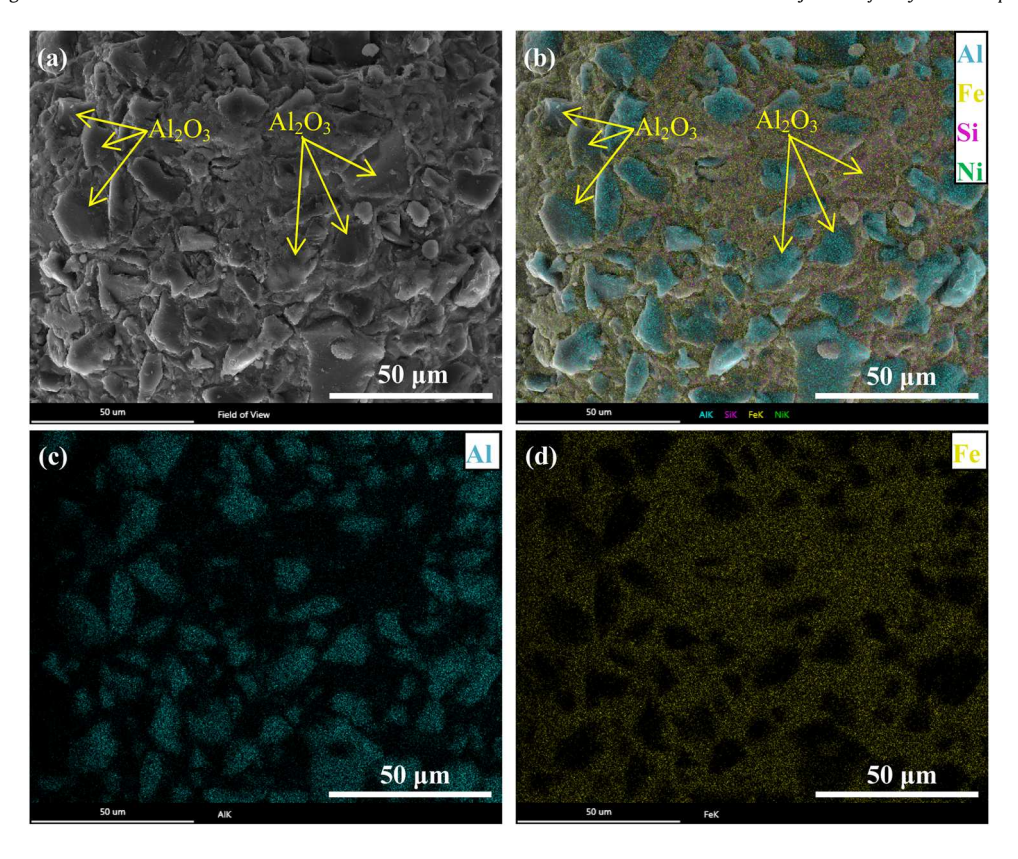


Fig. 7. (a) SEM image and (b-d) EDS analysis of MAP surface: (b) Al-Fe-Si-Ni, (c) Al, (d) Fe.

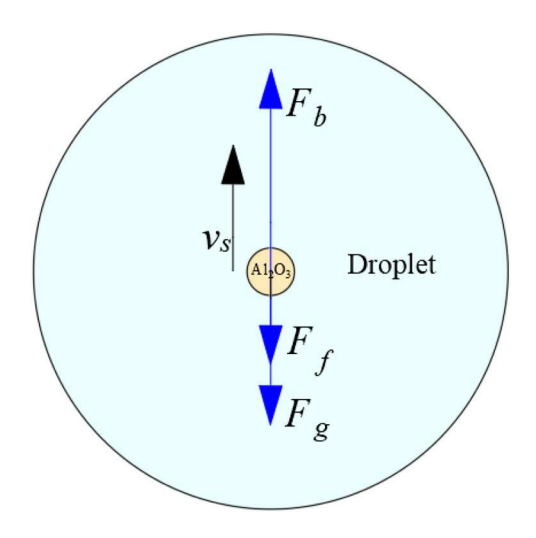


Fig. 8. The force analysis diagram of Al_2O_3 abrasive in the metal droplet.

The buoyancy (F_b) of Al_2O_3 abrasive in metal droplet can be expressed as:

$$F_b = \rho_l g V_s = \frac{4}{3} \pi \rho_l g r_s^3 \tag{11}$$

According to Stokes law, the internal friction resistance (F_f) of Al₂O₃ abrasive in metal droplet can be expressed as [27]:

$$F_f = 6\pi \eta_l r_s v_s \tag{12}$$

The resultant force (F_r) of Al_2O_3 abrasive in metal droplet can be expressed as:

$$F_r = F_b - F_g - F_f \tag{13}$$

Therefore, the acceleration of Al₂O₃ abrasive in metal droplet is:

$$a_{s} = \frac{F_{r}}{\rho_{s}V_{s}} = \frac{2\rho_{l}gr_{s}^{2} - 2\rho_{s}gr_{s}^{2} - 9\eta_{l}v_{s}}{2\rho_{s}r_{s}^{2}}$$
(14)

Then the time taken for the Al_2O_3 abrasive at the center of the droplet to move to the surface of the droplet is:

$$t_m = \sqrt{\frac{2r_l}{a_s}} \tag{15}$$

In the above equations, the density (ρ_l) of metal droplet is about 7 g/cm^3 , the density (ρ_s) of Al_2O_3 abrasive is 3.5 g/cm^3 , the gravitational acceleration (g) is 9.8 m/s^2 , the radius (r_s) of Al_2O_3 abrasive is 3.5 mm, and the average viscosity (η_l) of iron matrix at $1300-1600 \,^{\circ}\text{C}$ is about $0.008 \, \text{Pa-s} \, [28]$. If the Al_2O_3 abrasive is only affected by gravity and buoyancy when moving in the droplet, the average velocity (v_s) of the Al_2O_3 abrasive moving from the center to the surface of the droplet can be expressed as:

$$v_{s}' = \frac{r_{l}}{\sqrt{2\eta/a_{s}'}} = \frac{r_{l}}{\sqrt{2\eta/g}} \tag{16}$$

The velocity of Al_2O_3 abrasive in the actual movement process is not only affected by gravity and buoyancy, but also by the internal friction resistance of droplet. Therefore, the actual average velocity (v_s) of Al_2O_3 abrasive in the droplet is lower than v_s '. By substituting the above data into Eqs. (14)–(16), it can be calculated that the acceleration (a_s) of ceramic particle in the metal droplet with particle size of $100\,\mu\mathrm{m}$ is about $9.79\,\mathrm{m/s^2}$, and the time (t_m) taken for the Al_2O_3 abrasive at the center of the droplet to move to the surface of the droplet is about $0.0032\,\mathrm{s}$

In the process of preparing metal powder via gas atomization, the solidification of metal droplet follows Newton's law of cooling. The forms of droplet heat dissipation are convective heat dissipation and radiant heat dissipation, in which convective heat dissipation is the main form [29]. In gas-solid atomization, there is convective heat transfer not only between N_2 and metal droplet, but also between

Al₂O₃ abrasive and metal droplet. Therefore, the heat dissipation of metal droplet in the preparation of MAP via gas-solid atomization can be expressed as [30]:

$$Q = h_g A_g (T_l - T_g) + h_s A_s (T_l - T_s)$$
(17)

where h_g is the convective heat transfer coefficient between gas and droplet, A_g is the contact area between gas and droplet, T_l is the droplet temperature, T_g is the gas temperature, h_s is the convective heat transfer coefficient between Al_2O_3 abrasive and droplet, A_s is the contact area between Al_2O_3 abrasive and droplet, and T_s is the temperature of Al_2O_3 abrasive. The temperature of gas and Al_2O_3 abrasive is approximately the same after mixing, i.e. $T_g = T_s$. The contact area between Al_2O_3 abrasive and droplet is set as $A_s = \alpha A_g$. Then, Eq. (17) can be written as:

$$Q = hA_g(T_l - T_g) (18)$$

where $h = h_g + \alpha h_s$ is the comprehensive heat transfer coefficient of gas-solid two-phase flow and metal droplet. The cooling rate of metal droplet can be obtained from Newton's law of cooling [31]:

$$\frac{dT}{dt} = -\frac{3h(T_l - T_g)}{\rho_l C_l \eta} \tag{19}$$

where C_l is the specific heat capacity of metal droplet. Because the contact area (A_s) between Al_2O_3 abrasive and droplet and other parameters are difficult to predict, the cooling rate of metal droplet cannot be accurately calculated by Eq. (19). Therefore, the cooling rate (C_R) of metal droplet is estimated by measuring the secondary dendrite arm spacing (λ) of MAP. The relationship between secondary dendrite arm spacing and cooling rate can be expressed as [32]:

$$\lambda = 148(C_R)^{-0.38} \tag{20}$$

And we calculated that the average secondary dendrite arm spacing of MAPs with particle size of 100 µm is about 2.5 µm. By substituting $\lambda = 2.5$ into Eq. (20), it can be calculated that the cooling rate (C_R) is 4.6×10^4 °C/s. Then, the time taken for the metal droplet temperature to drop from 1600 °C to 1300 °C is about 0.0065 s. The cooling time (t_c = 0.0065) of droplet with particle size of 100 µm is about twice the time ($t_m = 0.0032$) of Al₂O₃ abrasive moving from the center to the surface of droplet. After that, the cooling time of MAPs with different particle sizes and the time of Al₂O₃ abrasive moving from the center to the surface of droplet were measured and calculated. The comparison results are shown in Fig. 9. The difference between cooling time (t_c) and moving time (t_m) gradually increases with the increase of MAP particle size. In the early stage of gas-solid atomization, when the Al₂O₃ abrasives initially break the liquid flow, the metal droplet diameter is large, and the cooling rate of the droplet is slow. Most of the Al₂O₃ abrasives have moved to the droplet surface before the droplet solidifies. Therefore, most MAPs have few Al₂O₃ abrasives inside. The few Al₂O₃ abrasives remaining inside the iron matrix are due to the fact that when the Al₂O₃ abrasives enter or move out of the droplet, the metal droplet has begun to solidify. Or the droplet diameter is small and the droplet solidifies quickly, so that the Al₂O₃ abrasives have no time to move to the droplet surface.

Therefore, during the preparation process of ceramic/metal composite spherical MAPs in MAF via gas-solid atomization, the cooling rate should not be too large, and the density difference between ceramic and metal should not be too small. It must be ensured that the Al₂O₃ abrasive has enough time to move from the inside of metal droplet to the surface, and the metal droplet also has enough spheroidization time. On the other hand, the cooling rate should not be too small either, and it must be ensured that the composite droplet has completely solidified before falling to the bottom of the atomizing chamber. After that, we want to prepare ceramic/metal

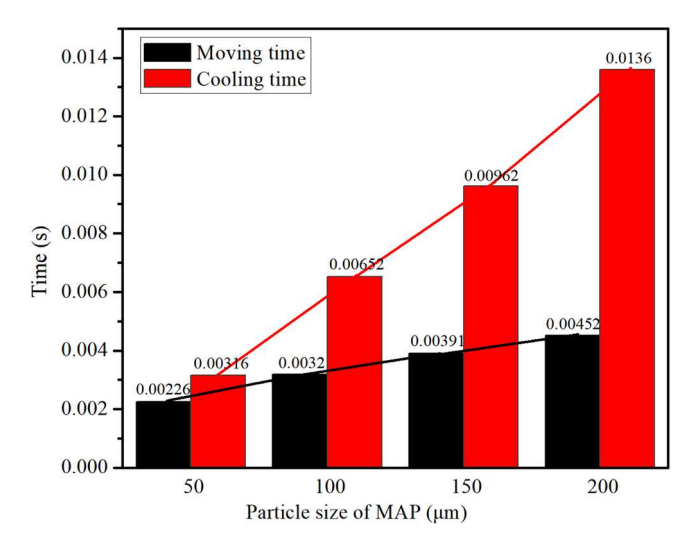


Fig. 9. Comparison of the time of Al_2O_3 abrasive moving from the center to the surface of droplets and the cooling time of droplets with different particle sizes.

composite spherical powders in 3D printing via gas-solid atomization, and the ceramic particles should be evenly distributed inside and on the surface of the powder. Therefore, when preparing ceramic/metal composite powders in 3D printing, it is necessary to increase the cooling rate or reduce the density difference between ceramic particle and metal droplet, so as to slow down the moving speed of ceramic particle in metal droplet.

4. Conclusions

In this study, the breaking mechanism and formation mechanism of ceramic/metal composite spherical MAPs prepared by gas-solid atomization were explored. The results are summarized as follows:

- 1. The breaking mechanism of gas-solid two-phase flow to molten metal is different from that of the pure gas to molten metal. When the molten metal is broken by pure gas, the droplets are stripped from the surface of the molten metal through the disturbance of gas, while the way that the molten metal is broken by the gas-solid two-phase flow is the disturbance breaking of gas, accompanied by the penetration breaking of ceramic abrasives. Under the same experimental conditions, the molten metal is easier to be broken by gas-solid two-phase flow, where the average diameter of droplets is smaller and the breaking efficiency is higher.
- 2. The MAP prepared by gas-solid atomization has good sphericity, with Al₂O₃ abrasives evenly and densely distributed on the surface of the iron matrix, and there are almost no Al₂O₃ abrasives inside the iron matrix, which is basically consistent with the ideal MAP model. Most Al₂O₃ abrasives on the surface of MAP are partially covered by iron matrix, and a few Al₂O₃ abrasives are completely covered by iron matrix.
- 3. After analyzing and calculating the movement process of Al₂O₃ abrasive in metal droplet and the cooling process of metal droplet, it is found that the time for most Al₂O₃ abrasives in droplet to move to the surface of droplet is less than the solidification time of droplet. Therefore, the ceramic/metal composite spherical MAP prepared by gas-solid atomization is closer to the ideal MAP.
- 4. This study reveals the breaking mechanism of gas-solid twophase flow to molten metal and the formation mechanism of ceramic/metal composite spherical MAP, which provides theoretical support and method guidance for the development of ceramic/metal composite MAPs in MAF and ceramic/metal

composite powders in 3D printing prepared by gas-solid atomization.

CRediT authorship contribution statement

Linzhi Jiang: Methodology, Software, Investigation, Writing – Original Draft. **Tieyan Chang**: Writing – Review & Editing, Visualization. **Guixiang Zhang**: Conceptualization, Supervision. **Yugang Zhao**: Validation, Formal analysis. **Haoxin Chen**: Software, Formal analysis. **Ning Liu**: Investigation. **Xue Liu**: Data Curation.

Data availability

The data that has been used is confidential.

Declaration of Competing Interest

The authors declare that they have no known competing financial interests or personal relationships that could have appeared to influence the work reported in this paper.

Acknowledgment

This work is supported by the National Natural Science Foundation of China (No. 51675316). NSF's ChemMatCARS Sector 15 is supported by the Divisions of Chemistry (CHE) and Materials Research (DMR), National Science Foundation, under grant number NSF/CHE- 1834750.

References

- [1] A. Misra, P.M. Pandey, U.S. Dixit, Modeling of material removal in ultrasonic assisted magnetic abrasive finishing process, Int. J. Mech. Sci. 131–132 (2017) 853–867, https://doi.org/10.1016/j.ijmecsci.2017.07.023
- [2] H. Yamaguchi, J. Kang, F. Hashimoto, Metastable austenitic stainless steel tool for magnetic abrasive finishing, CIRP Ann.-Manuf. Technol. 60 (2011) 339–342, https://doi.org/10.1016/j.cirp.2011.03.119
- [3] J.S. Kwak, Enhanced magnetic abrasive polishing of non-ferrous metals utilizing a permanent magnet, Int. J. Mach. Tool. Manuf. 48 (2009) 613–618, https://doi. org/10.1016/j.ijmachtools.2009.01.013
- [4] L.D. Heng, J.S. Kim, J.F. Tu, S.D. Mun, Fabrication of precision meso-scale diameter ZrO₂ ceramic bars using new magnetic pole designs in ultra-precision magnetic abrasive finishing, Ceram. Int. 46 (2020) 17335–17346, https://doi.org/10.1016/j. ceramint 2020 04 022
- [5] W.H. Li, X.H. Li, S.Q. Yang, W.D. Li, A newly developed media for magnetic abrasive finishing process: material removal behavior and finishing performance, J. Mater. Process. Technol. 260 (2018) 20–29, https://doi.org/10.1016/j. jmatprotec.2018.05.007
- [6] Y. Wang, D.J. Hu, Study on the inner surface finishing of tubing by magnetic abrasive finishing, Int. J. Mach. Tool. Manuf. 45 (2005) 43–49, https://doi.org/10. 1016/j.ijmachtools.2004.06.014
- [7] Z.Q. Liu, Y. Chen, Y.J. Li, X. Zhang, Comprehensive performance evaluation of the magnetic abrasive particles, Int. J. Adv. Manuf. Technol. 68 (2013) 631–640, https://doi.org/10.1007/s00170-013-4783-6
- [8] C.J. Wang, C.F. Cheung, L.T. Ho, K.L. Yung, L.B. Kong, A novel magnetic field-assisted mass polishing of freeform surfaces, J. Mater. Process. Technol. 279 (2020) 116552, https://doi.org/10.1016/j.jmatprotec.2019.116552
- [9] A.C. Wang, S.J. Lee, Study the characteristics of magnetic finishing with gel abrasive, Int. J. Mach. Tool. Manuf. 49 (2009) 1063–1069, https://doi.org/10.1016/ j.ijmachtools.2009.07.009

- [10] K. Hanada, H. Yamaguchi, H. Zhou, New spherical magnetic abrasives with carried diamond particles for internal finishing of capillary tubes, Diam. Relat. Mater. 17 (2008) 1434–1437, https://doi.org/10.1016/j.diamond.2008.01.100
- [11] W.S. Li, J.J. Li, B. Cheng, X.J. Zhang, Achieving in-situ alloy-hardening core-shell structured carbonyl iron powders for magnetic abrasive finishing, Mater. Des. 212 (2021) 110198. https://doi.org/10.1016/j.matdes.2021.110198
- L.Z. Jiang, G.X. Zhang, J.J. Du, P.X. Zhu, T.L. Cui, Y.T. Cui, Processing performance of Al2O3/Fe-based composite spherical magnetic abrasive particles, J. Magn. Magn. Mater. 528 (2021) 167811, https://doi.org/10.1016/j.jmmm.2021.167811
 G.W. Chang, B.H. Yan, R.T. Hsu, Study on cylindrical magnetic abrasive finishing
- [13] G.W. Chang, B.H. Yan, R.T. Hsu, Study on cylindrical magnetic abrasive finishing using unbonded magnetic abrasives, Int. J. Mach. Tool. Manuf. 42 (2002) 575–583, https://doi.org/10.1016/S0890-6955(01)00153-5
- [14] X.X. Tan, S.Y. Wang, Y. Chen, Y.W. Zhou, Z. Li, Design, preparation and characterization of iron nitride magnetic abrasives, J. Alloy. Compd. 774 (2019) 443–450, https://doi.org/10.1016/j.jallcom.2018.09.389
- [15] G.X. Zhang, Y.G. Zhao, D.B. Zhao, F.S. Yin, Z.D. Zhao, Preparation of white alumina spherical composite magnetic abrasive by gas atomization and rapid solidification, Scr. Mater. 65 (2011) 416–419, https://doi.org/10.1016/j.scriptamat.2011.05. 021
- [16] G.X. Zhang, Y.G. Zhao, D.B. Zhao, D.W. Zuo, F.S. Yin, New iron-based SiC spherical composite magnetic abrasive for magnetic abrasive finishing, Chin. J. Mech. Eng.-Engl. Ed. 26 (2013) 377–383, https://doi.org/10.3901/CJME.2013.02.377
- [17] L.Z. Jiang, T.Y. Chang, P.X. Zhu, G.X. Zhang, J.J. Du, N. Liu, H.X. Chen, Influence of process conditions on preparation of CBN/Fe-based spherical magnetic abrasive via gas atomization, Ceram. Int. 47 (2021) 31367–31374, https://doi.org/10.1016/ iant 2020.01.036
- [18] Y.W. Gao, Y.G. Zhao, G.X. Zhang, F.S. Yin, G.Y. Zhao, H. Guo, Preparation and characterization of spherical diamond magnetic abrasive powder by atomization process, Diam. Relat. Mater. 102 (2020) 107658, https://doi.org/10.1016/j. diamond.2019.107658
- [19] S.A. Sajjadi, M. Torabi Parizi, H.R. Ezatpour, A. Sedghi, Fabrication of A356 composite reinforced with micro and nano Al₂O₃ particles by a developed compocasting method and study of its properties, J. Alloy. Compd. 511 (2012) 226–231, https://doi.org/10.1016/j.jallcom.2011.08.105
- [20] M. Ao, H.M. Liu, C.F. Dong, S. Feng, J.C. Liu, Degradation mechanism of 6063 aluminium matrix composite reinforced with TiC and Al₂O₃ particles, J. Alloy. Compd. 859 (2021) 157838, https://doi.org/10.1016/j.jallcom.2020.157838
- [21] P. Gupta, N. Ahamad, J. Mehta, D. Kumar, M.A. Quraishi, Corrosion, optimization and surface analysis of Fe-Al₂O₃-CeO₂ metal matrix nanocomposites, Proc. Inst. Mech. Eng. C-J. Mec. 236 (2022) 4346–4356, https://doi.org/10.1177/ 09544062211047844
- 221 G.Z. Chen, The State of Matter, Science Press, Beijing, 1985.
- [23] P. Emerson, J. Crockett, D. Maynes, Thermal atomization during droplet impingement on superhydrophobic surfaces: influence of Weber number and micropost array configuration, Int. J. Heat Mass Transf. 164 (2021) 120559, https://doi.org/10.1016/j.iiheatmasstransfer.2020.120559
- [24] N. Blanken, M.S. Saleem, C. Antonini, M.J. Thoraval, Rebound of self-lubricating compound drops, Sci. Adv. 6 (2020), https://doi.org/10.1126/sciadv.aay3499 eaav3499.
- [25] G. Chen, X. Yang, B. Su, C.J. Tu, Criterion of gas and solid dual-phase flow atomization crash in molten metal, Trans. Nonferr. Metal. Soc. 24 (2016) 208–216, https://doi.org/10.1016/S1003-6326(14)63049-1
- [26] A.M. Podvysotsky, A.A. Shraiber, Coalescence and break-up of drops in twophase flows, Int. J. Multiphas. Flow. 10 (1984) 195–209, https://doi.org/10.1016/ 0301-9322(84)90017-X
- [27] O. Gutiérrez-Varela, R. Santamaria, Molecular nature of the drag force, J. Mol. Liq. 338 (2021) 116466, https://doi.org/10.1016/j.molliq.2021.116466
- [28] Z.I. Morita, T. Iida, Viscosity of molten iron and steel, Iron. Steel 02 (1982) 54–61, https://doi.org/10.13228/j.boyuan.issn0449-749x.1982.02.012
- [29] T.W. Clyne, Numerical treatment of rapid solidification, Metall. Mater. Trans. B 15 (1984) 369–381, https://doi.org/10.1007/BF02667341
- [30] P. Mathur, S. Annavarapu, D. Apelian, A. Lawley, Spray casting: an integral model for process understanding and control, Mater. Sci. Eng. A 142 (1991) 261–276,
- https://doi.org/10.1016/0921-5093(91)90665-A

 [31] P.S. Grant, B. Cantor, L. Katgerman, Modelling of droplet dynamic and thermal histories during spray forming—I. individual droplet behaviour, Acta Mater. 41 (1993) 3097–3108, https://doi.org/10.1016/0956-7151(93)90039-U
- [32] M. El-Bealy, B.G. Thomas, Prediction of dendrite arm spacing for low alloy steel casting processes, Metall. Mater. Trans. B 27 (1996) 689–693, https://doi.org/10. 1007/BF02915668